JOURNAL OF THERMOPHYSICS AND HEAT TRANSFER
Vol. 20, No. 3, July–September 2006

Heat Transfer in Two-Pass Rotating Rectangular Channels (AR = 2:1) with Discrete Ribs

Wen-Lung Fu,* Lesley M. Wright,* and Je-Chin Han†
Texas A&M University, College Station, Texas 77843-3123

This paper reports the heat transfer coefficients and friction factors in a two-pass rotating rectangular channel with ribs, applicable to an internally cooled turbine blade. The channel aspect ratio is 2:1. Five different turbulators are studied: 45-deg angled ribs, V-shaped ribs, discrete 45-deg angled ribs, discrete V-shaped ribs, and crossed V-shaped ribs. The ribs are placed on the leading and trailing surfaces. The Reynolds number ranges from 5000 to 40,000. The corresponding rotation numbers vary from 0.206 to 0.026 for a fixed rotation speed of 550 rpm. The rib-height-to-hydraulic-diameter ratio (e/D) is 0.094, the rib-pitch-to-height ratio (P/e) is 10, and the inlet-coolant-to-wall-density ratio ($\Delta\rho/\rho$) is maintained around 0.115. For each case, two channel orientations with respect to the plane of rotation are studied, 90 and 135 deg. The results show that the V-shaped ribs and discrete V-shaped ribs have higher heat transfer enhancement than the 45-deg angled ribs and discrete 45-deg angled ribs for both rotating and nonrotating cases. The pressure measurements show the 45-deg angled ribs incurred the highest frictional losses. Based on the present study, the discrete V-shaped ribs have the best overall thermal performance in both rotating and nonrotating channels.

Nomenclature

A	=	area of smooth wall
A_c	=	cross-sectional area of the channel
AR	=	aspect ratio, W/H
Bo	=	buoyancy parameter, $(\Delta\rho/\rho)Ro^2(R/D)$
D	=	hydraulic diameter, $4A_c/Per$
e	=	rib height
f	=	friction factor
f_o	=	Blasius fully developed friction factor in nonrotating smooth tube
H	=	channel height
h	=	heat transfer coefficient
k	=	thermal conductivity of coolant
L	=	heated length of the channel
Nu	=	local Nusselt number, hD/k
Nu_o	=	Nusselt number for fully developed turbulent flow in smooth pipe
P	=	rib pitch
P_e	=	pressure at the exit of the channel
Per	=	channel perimeter
P_i	=	pressure at the inlet of the channel
Pr	=	Prandtl number
q	=	heat transfer rate at wall
R	=	mean rotating radius
Re	=	Reynolds number, $\rho VD/\mu$
Ro	=	rotation number, $\Omega D/V$
T_b	=	local coolant temperature
T_w	=	wall temperature
V	=	bulk velocity in streamwise direction
W	=	channel width
α	=	rib angle
β	=	angle of channel orientation with respect to the axis of rotation
$(\Delta\rho/\rho)$	=	inlet-coolant-to-wall-density ratio, $(T_w - T_{bi})/T_w$
μ	=	dynamic viscosity of coolant
ρ	=	density of coolant
Ω	=	rotational speed

Received 14 August 2005; accepted for publication 30 November 2005.

*Graduate Research Assistant, Turbine Heat Transfer Laboratory, Department of Mechanical Engineering.

†M.C. Easterling Chair Professor, Turbine Heat Transfer Laboratory, Department of Mechanical Engineering; jc-han@tamu.edu. Associate Fellow AIAA.

Introduction

TO improve thermal efficiency, advanced gas turbines operate at high temperatures. The high inlet temperature creates thermal stresses on the blades, which can be detrimental to the operation of the engine. To achieve reasonable durability goals, improved cooling techniques are applied to turbine blades. Internal cooling is one of the most effective techniques used in current turbine-blade design. Internal cooling is achieved by circulating compressed air in multipass flow channels inside the blade structure. To increase the heat transfer within the internal cooling channels, the internal surfaces usually are roughened by angled ribs to trip the boundary layer and increase turbulence. As the turbine blade rotates, the Coriolis force directs the coolant to the trailing wall in the channel's radial outward flow. Therefore, heat transfer is enhanced on the trailing wall and reduced on the leading wall in the channel with radial outward flow with rotation. The Coriolis force acts in the opposite direction in a rotating channel with radial inward flow; as a result, the heat transfer is enhanced on the leading wall and reduced on the trailing wall. A comprehensive review of turbine-blade internal cooling can be found in the book by Han et al.[1]

Earlier studies on cooling passages were primarily based on one-pass stationary models that can study the channel aspect ratio effect and surface roughness effect. The one-pass model did not include the turn effect, which is a significant parameter in a multipass flow channel. Also, the stationary models neglect the Coriolis and buoyancy effects, which alter the velocity, turbulence, and temperature distributions. Metzger and Sahm[2] are pioneers who studied heat transfer in the multi-pass flow channels. They studied forced convection in a two-pass smooth rectangular channel by varying the divider location and the gap at the 180-deg turn. Fan and Metzger[3] extended the work by Metzger and Sahm[2] by varying the channel width. They concluded that increasing the channel aspect ratio results in smaller azimuthal heat transfer variations and increases overall channel heat transfer. Han et al.[4] studied the local heat/mass transfer distribution in a non-rotating two-pass ribbed channel. Han and Zhang[5] studied the effect of rib-angle orientation on the local heat/mass transfer distribution in a nonrotating three-pass rib-roughened channel. It was observed that the rib angle, the rib orientation, and the sharp 180-deg turn significantly affect the local heat/mass transfer

distributions. Han et al.[6] studied the effect of the rib-angle orientation on heat transfer distributions and pressure drop in a nonrotating square channel with opposite, parallel ribbed walls. They found that the 60-deg and 45-deg V-shaped ribs perform better heat transfer than the 60-deg and 45-deg parallel ribs and 90-deg transverse ribs. Park et al.[7] studied the effects of rib angle on five different aspect ratio rectangular ducts under nonrotating conditions. They found the order of heat transfer enhancement for the low-aspect-ratio ducts ($AR = 1{:}1$, 1:2, and 1:4) is 60-deg, 45-deg, and 30-deg/90-deg angled ribs. For the high-aspect-ratio ducts ($AR = 2{:}1$ and 4:1), the augmentation order is 90-deg/60-deg, 45-deg, and 30-deg angled ribs. Taslim et al.[8] used liquid crystal techniques to study different rib configurations in a one-pass square duct. They concluded that the V-shaped ribs have higher heat transfer enhancement and friction factors than the angled ribs. Ekkad and Han[9] also used a liquid crystal technique to perform a detailed study on heat transfer characteristics in a nonrotating square channel with a sharp 180-deg turn. One wall of the channel had periodically placed rib turbulators. The rib configurations studied were 90-deg parallel, 60-deg parallel, 60-deg V-shaped, and 60-deg inverted V-shaped ribs. Cho et al.[10] presented mass transfer measurements in a one-pass nonrotating duct ($AR = 2.04{:}1$) with different rib arrangements. Their results show that discrete 90-deg angled ribs have better heat transfer enhancement than nondiscrete 90-deg angled ribs. However, the discrete and nondiscrete 45-deg angled ribs have similar heat transfer enhancement.

All of the above studies are for nonrotating channels. It has been shown for nonrotating channels that the angled ribs have better heat transfer than normal ribs (90-deg), and the V-shaped ribs have better heat transfer than the angled ribs.

Wagner et al.[11,12] conducted a detailed experimental study to determine the effects of rotation (Coriolis and buoyancy forces) on the local heat transfer of a multipass square channel with smooth walls. They concluded that the rotation resulted in different heat transfer on the leading and the trailing surfaces in the first pass; the leading surface experienced decreased heat transfer, whereas the trailing surface experienced an enhancement in heat transfer. In the second pass, the heat transfer on the leading and the trailing surfaces was opposite due to the reversal of the Coriolis force direction. Taslim et al.[13,14] investigated the heat transfer distribution in one-pass square and rectangular rib-roughened channels under rotation. They found that the effects of rotation were more apparent in rib-roughened channels with a larger channel aspect ratio and a lower rib blockage ratio. Han et al.[15] investigated the uneven wall temperature effect on local heat transfer in a rotating two-pass square channel with smooth walls. They concluded that uneven surface temperatures on the leading and trailing surfaces create unequal local buoyancy forces, which alter heat transfer coefficients. Parsons et al.[16] studied the effects of channel orientation and wall heating on the local heat transfer coefficients in a rotating two-pass square channel with ribbed walls. They found that the effects of the Coriolis force and cross-stream flow were reduced as the channel orientation changed from the normal $\beta = 90$ deg to an angled orientation of $\beta = 135$ deg. Zhang et al.[17] analyzed the heating condition effects in a two-pass square duct with angled rib turbulators with rotation. They found that an uneven wall temperature had a significant impact on the local heat transfer coefficients. Dutta and Han[18] also investigated the local heat transfer coefficients in rotating smooth and ribbed two-pass square channels with three channel orientations. In addition, Park and Lau[19] and Park et al.[20] conducted experimental work using naphthalene sublimation to study the effects of the Coriolis force, 180-deg turn, channel orientation, and different rib arrangements on local heat/mass transfer distributions on the leading and trailing walls of a two-pass square channel. Liou et al.[21] performed heat transfer measurements using a liquid crystal technique in a rotating two-pass square duct with 90-deg in-line ribs. Their results are comparable with those of Parson's et al.[16] Al-Hadhrami and Han[22] studied the rotation effect on heat transfer in a rotating two-pass square duct with five different arrangements of 45-deg angled rib turbulators. They concluded that the parallel rib orientation (ribs in first and second passes are parallel and ribs on leading and trailing walls are parallel) provides a higher overall Nusselt number ratio than the crossed rib orientation, particularly for increasing rotation numbers.

Almost all of the rotating studies have focused on square or close-to-square ducts. Recently, studies have moved to rotating rectangular ducts. The effect of rotation on the heat transfer distribution in a rotating, rectangular ($AR = 2{:}1$) two-pass channel with rib-roughened walls was investigated by Azad et al.[23] They showed that the heat transfer coefficients decrease from the leading wall and increase from the trailing wall in the first pass. They also concluded that the effect of rotation is more apparent in the channel oriented at 90 deg than the channel oriented at 135 deg with respect to the direction of rotation.

Single-pass rectangular ($AR = 4{:}1$) channels were studied by Griffith et al.[24] They concluded that this narrow rectangular passage creates more heat transfer enhancement than the smaller aspect ratio channels. They also found that significant spanwise variation is present across the width of the channel, and this variation is amplified by the use of angled ribs. Lee et al.[25] also investigated six different rib configurations in single-pass rectangular ($AR = 4{:}1$) channels. They found that the V-shaped ribs produce the greatest heat transfer enhancement in both rotating and nonrotating channels. They also confirmed the finding of Griffith et al.[24] significant spanwise variation is present in the channels with angled ribs, but this variation decreases in the channels with V-shaped ribs. Al-Hadhrami et al.[26] studied the effect of rotation on heat transfer in rotating two-pass rectangular channels ($AR = 2{:}1$) with rib turbulators for two channel orientations. They found that the parallel V-shaped ribs produce better heat transfer enhancement than the crossed V-shaped ribs and inverted V-shaped ribs. Furthermore, they confirmed the conclusion from Azad et al.[23] that the 90-deg channel orientation produces a greater rotating effect on heat transfer than a 135-deg channel orientation.

Cho et al.[27] used a mass transfer method to study the effect of rotation in a rotating two-pass rectangular channel ($AR = 1{:}2$) with 70-deg angled ribs. Their results showed that the rotation effect diminished in the second pass due to the 180-deg turn effect. An experimental result for a 1:4 rotating two-pass channel was reported by Agarwal et al.[28] using the mass transfer method. For a smooth surface, they found that the 1:4 channel has lower heat/mass transfer than the square channel. For the 90-deg ribbed walls, the Sherwood number ratio shows a decreasing trend with increasing Reynolds number. Fu et al.[29] studied the channel-aspect-ratio effect in rotating two-pass-low-aspect ratio ($AR = 1{:}2$ and $AR = 1{:}4$) ducts with 45-deg angled rib turbulators. Their results also showed that the rotation effect diminished in the second pass, which was also reported by Cho et al.[27] Wright et al.[30] studied the heat transfer distributions in a one-pass rotating rectangular duct ($AR = 4{:}1$) with angled, V-shaped, and W-shaped rib turbulators. They concluded that the discrete V-shaped and discrete W-shaped ribs have the best thermal performance in both rotating and nonrotating cases.

From this research, it has been shown that the V-shaped ribs have better heat transfer enhancement than the angled ribs for rotating and non-rotating channels. Discrete ribs are better than nondiscrete ribs in nonrotating and rotating channels with radial outward flow (Wright et al.,[30] $AR = 4{:}1$). However, Cho et al.[10] showed a different result in a 2.04:1 channel. Their discrete ribs have slightly lower heat transfer than nondiscrete ribs. Turbine blade designers need to know if the discrete ribs yield more heat transfer enhancement than the nondiscrete ribs. Will the aspect ratio affect the heat transfer on the discrete ribs and the nondiscrete ribs? What is the performance of the discrete and the nondiscrete ribs in multipass rotating channels? From the literature, there are limited data available to answer these questions. Therefore, this study investigated the effect of the discrete ribs and nondiscrete ribs on heat transfer enhancement in a rotating two-pass channel. The experiments were conducted in a 2:1 channel. Due to geometrical constraints, the 2:1 channel is more applicable than the 4:1 channel as a multipass channel for turbine blades. Also, it has wider walls than conventional square channels, so more complicated configurations can be considered. Two main rib arrangements were chosen to study the heat transfer enhancement due to discrete and nondiscrete configurations; these two more

advanced rib arrangements are 45-deg angled ribs and V-shaped ribs. These ribs are placed parallel on the leading and the trailing walls. In addition to these four rib arrangements, a crossed V-shaped rib is proposed in this study. This rib configuration is arranged in such a way that the rib-induced secondary flow can strengthen the rotation-induced vortices. All of these rib configurations have a rib angle of 45-deg to mainstream flow. This study provides more complete data on the comparison of discrete and nondiscrete ribs in a rotating two-pass rectangular channel.

Experimental Facility

The experimental test rig is shown in Fig. 1. A variable-frequency motor is connected via a gear-and-belt mesh to a hollow, rotating shaft. This shaft runs from the base of the test rig to the work platform and is attached orthogonal to the hollow, rotating arm. The test section is inserted inside the hollow rotating arm, which rotates in a plane orthogonal to the rotating shaft. The rotation speed of the arm is measured using a handheld optical tachometer. Thermocouple and heater wires are connected to a slip-ring assembly mounted to the rotating shaft. A 48-channel Scanivalve pressure transducer is mounted on the top of the rotating shaft. The signals of the thermocouples and pressure transducer are transferred to a data acquisition system through the slip ring. Power input to the heaters from the variable transformers is also transmitted through the slip-ring assembly. Cooling air is pumped from a steady-flow compressor, through an ASME orifice flow meter, then through the hollow rotating shaft, turning 90 deg and passing into the rotating arm, then through the test section, and finally is expelled into the atmosphere.

The geometry of the test section is shown in Fig. 2. The test section contains two passes connected by a 180-deg sharp turn. The channel is 25.4 × 12.7 mm in cross section with a hydraulic diameter (D) of 16.93 mm. The test section contains a 222.25-mm unheated entrance length to provide a hydrodynamic fully developed flow condition. Each pass has a 152.4-mm-long heating section. The clearance of the 180-deg sharp turn is 25.4 mm from tip to end wall. The divider wall has a thickness of 12.7 mm with a 6.35-mm radius at the tip. Cooling air is expelled to the atmosphere through a 6.35-mm-radius hole in the second pass. The distance from the end of the heated section in the second pass to the exit hole is 152.4 mm. The mean rotating radius is 635 mm.

A cross-sectional view of the test section is shown in Fig. 3. Each pass is divided into six segments. Each segment contains four copper plates: one for each wall. The inner wall has only five segments in the flow direction because of the 180-deg turn. The copper plates are

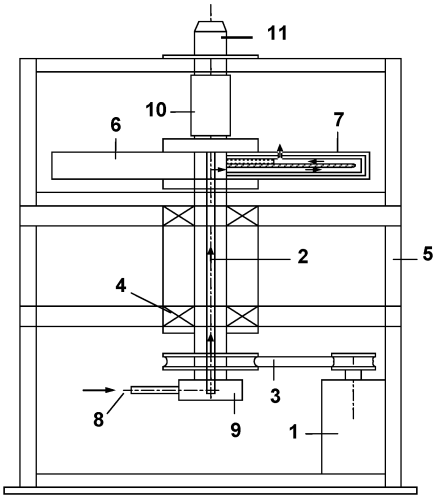

1. Electrical Motor with Controller
2. Rotating Shaft
3. Belt Drive Pulley System
4. Bearing Support System
5. Steel Table
6. Rotating Arm
7. Test Section
8. Compressor Air
9. Rotary Seal
10. Slip Ring
11. Pressure Transducer

Fig. 1 Schematic of the test rig.

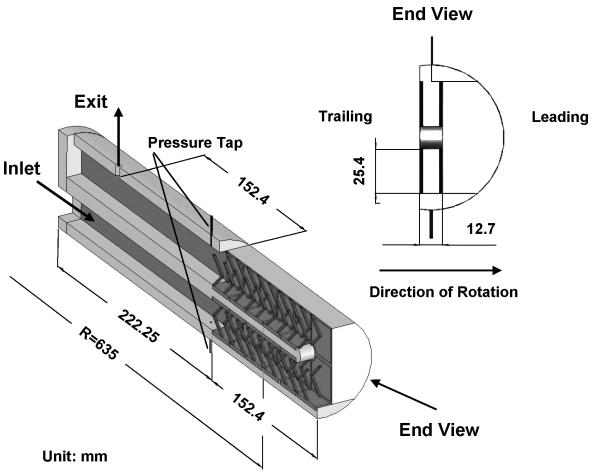

Fig. 2 Geometry of the test section (V-shaped ribs).

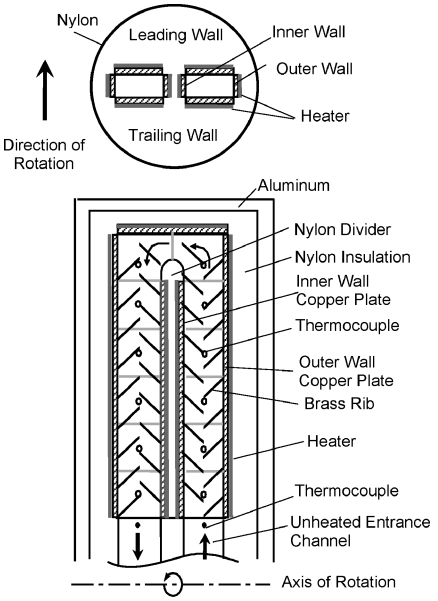

Fig. 3 Cross-sectional view of the test section.

mounted in a nylon substrate, which composes the bulk of the test section. Prefabricated flexible heaters are installed beneath the copper plates. All heaters supply steady, uniform heat flux to the copper plates. Sufficient power is supplied in order to maintain a maximum wall temperature of nearly 65°C for the corresponding section. This corresponds to an inlet coolant-to-wall density (temperature) ratio ($\Delta\rho/\rho$) of 0.115 for every test. Thermal conducting paste is applied between the heater and copper plates to promote heat transfer from the heater to the plates. Each 3.18-mm-thick copper plate has a 1.59-mm-deep blind hole drilled in the backside in which a copper–constantan thermocouple is installed 1.59 mm from the plate surface with thermal conducting glue. Thin nylon strips (1.59 mm) between the copper plates reduce the conduction effect between the plates.

Static pressure taps are used to measure the pressure of the coolant at the inlet and exit of the test section under isothermal conditions. The pressure taps are placed on the outer surface, which is normal to the leading and the trailing surfaces. The distance is 12.7 mm before the first copper plate and 12.7 mm after the last copper plate for the inlet and exit pressure taps, respectively. Each pressure tap is connected to a separate channel of the Scanivalve pressure transducer. From the calibration of the transducer with a standard U-tube manometer, the voltage signals obtained from the Scanivalve give the gauge pressure at both the inlet and exit of the test section. From these measurements, the total pressure drop incurred in the test section can be determined.

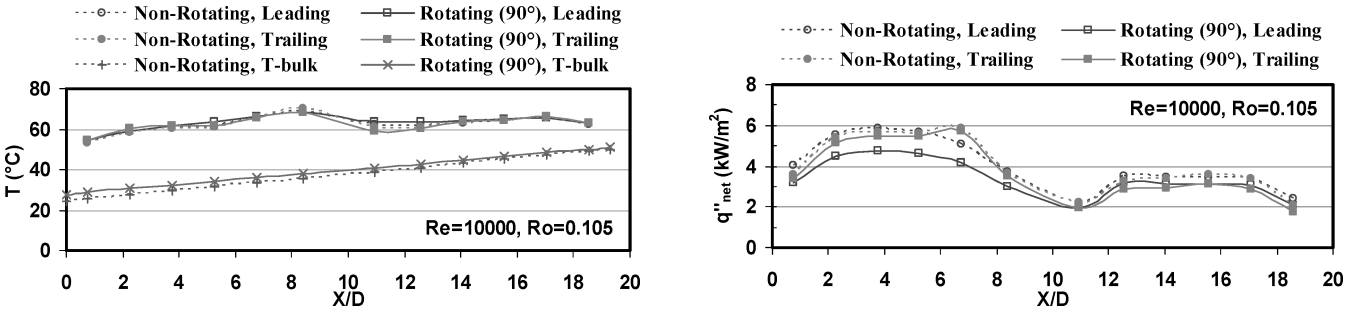

a) b)

Fig. 4 Typical temperature and net heat flux distributions (case (c), V-shaped ribs).

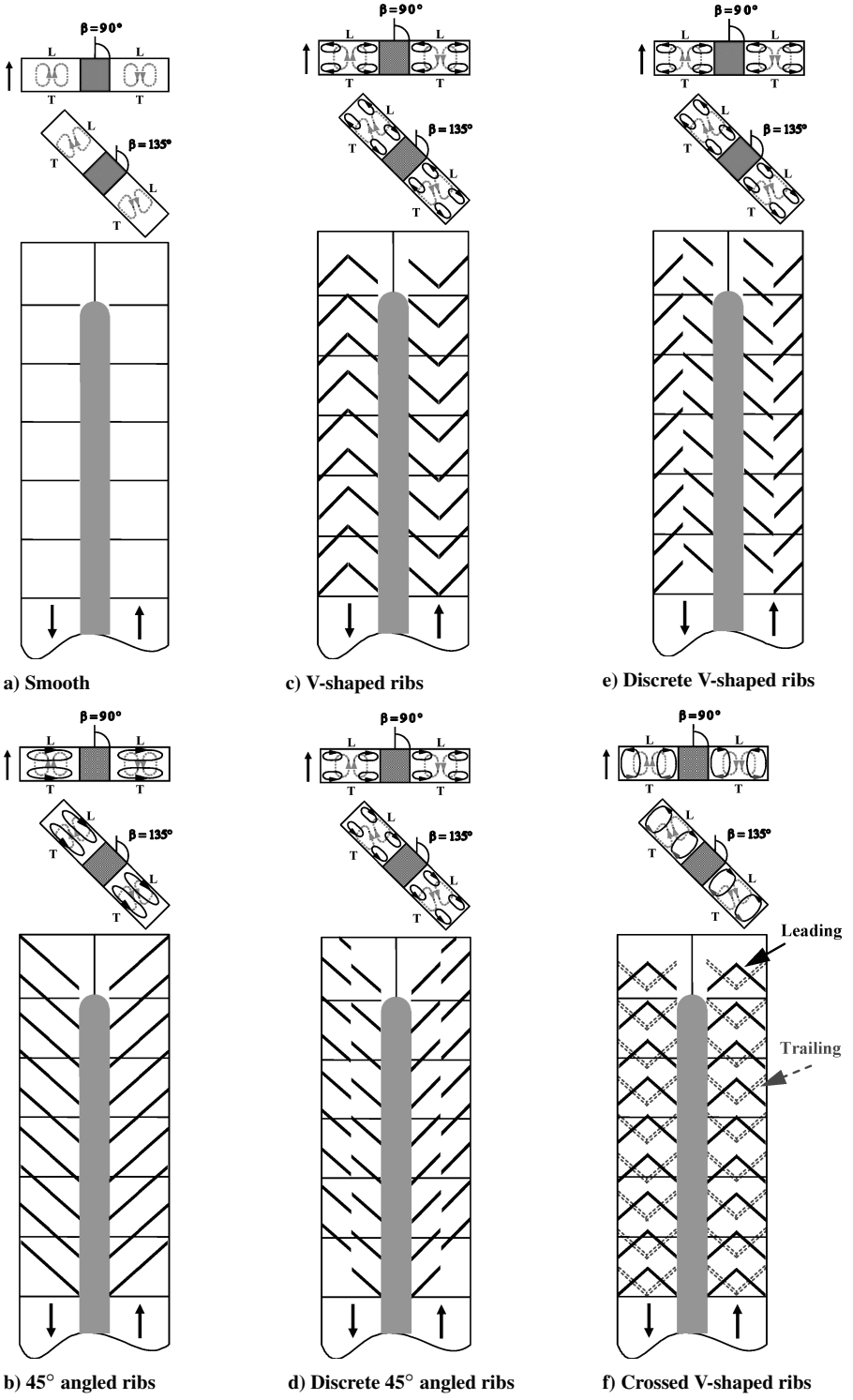

a) Smooth c) V-shaped ribs e) Discrete V-shaped ribs

b) 45° angled ribs d) Discrete 45° angled ribs f) Crossed V-shaped ribs

Fig. 5 Rib configurations and conceptual views of the secondary flow vortices induced by rotation (dashed line) and induced by ribs (solid line).

The ribs made of brass with a 1.59×1.59-mm cross section are glued on to the leading and trailing walls. A thin layer of conductive glue is used so that the thermal resistance between the brass ribs and the copper plates is negligible. The ratio of rib pitch to rib height is 10. The entire test duct is surrounded by insulating nylon material and fits in a hollow cylindrical aluminum alloy arm for structural rigidity. The experiments were conducted for Reynolds numbers 5, 10, 25, and 40×10^3. The test section rotates at a speed of 550 rpm, resulting in a range of rotation number (Ro) of approximately 0.026–0.206.

Data Reduction

The regionally averaged heat transfer coefficient was calculated by dividing the net heat input to the coolant by the projected area and the temperature difference between the copper plate and air bulk mean temperature:

$$h = \frac{q - q_{\text{loss}}}{A \times (T_w - T_b)} \tag{1}$$

Figure 4 shows the temperature distribution and net heat flux distribution on the leading and trailing surfaces for V-shaped ribs at $Re = 10 \times 10^3$. The net heat transfer rate is the electrical power supplied to the heater ($q = VI$) minus heat losses. Heat losses were determined by supplying power to the test section until a steady state condition was achieved in a no-flow condition. Fiberglass insulation was inserted into the test channel to prevent convection between the channel walls. This was done for several power inputs to obtain a relation between the total heat loss from each wall and the corresponding wall temperature. At a Reynolds number of 5×10^3, heat losses account for as much as 30% of the heat put into the test section. However at the highest Reynolds number of 40×10^3, just less than 10% of the heat input is lost by conduction through the test section.

To place the results on a common basis, the heat transfer area used in Eq. (1) was always that of a smooth wall (only the projected area of the ribs). The regionally averaged wall temperature is obtained from thermocouples that are embedded in each copper plate. The maximum wall temperature is 65°C. The bulk mean air inlet and exit temperatures are measured by thermocouples. The local bulk mean temperature (T_b) used in Eq. (1) is calculated from the linear interpolation between the measured inlet and exit bulk air temperatures. Another way to obtain the local bulk mean air temperature is using the energy balance through the test channel. The difference between the linear interpolation and energy balance of bulk mean temperature is 1 to 2°C in all cases.

The regionally averaged Nusselt number is normalized by the Nusselt number for fully developed turbulent flow in a smooth nonrotating circular pipe to reduce the influence of the flow Reynolds number on the heat transfer coefficient. The regionally averaged Nusselt number normalized by the Dittus–Boelter/McAdams correlation is

$$\frac{Nu}{Nu_o} = \frac{hD}{k_{\text{air}}} \frac{1}{(0.023\, Re^{0.8} Pr^{0.4})} \tag{2}$$

The Prandtl number (Pr) for air is 0.71. Air properties are taken based on the mean bulk air temperature.

The frictional losses in the cooling channel are determined by measuring the pressure drop from the inlet to the outlet of the test section. The friction factor is calculated using the measured inlet and exit pressures as shown in Eq. (3):

$$f = \frac{P_i - P_o}{4\left(L/D_h\right)\left(\frac{1}{2}\rho V^2\right)} \tag{3}$$

The friction factor ratio can then be calculated by dividing the friction factor by the turbulent friction factor in a smooth tube as given by the Blasius equation. This ratio is shown in Eq. (4):

$$f/f_o = f/(0.079\, Re^{0.25}) \tag{4}$$

Based on the heat transfer enhancement (Nu/Nu_o) and the pressure loss penalty (f/f_o), the thermal performance, η, of each rib configuration can be calculated. Equation (5) shows the thermal performance based on the constant pumping power condition as used by Han et al.[31]:

$$\eta = (Nu/Nu_o)/(f/f_o)^{\frac{1}{3}} \tag{5}$$

The estimated uncertainty for temperature measurement is 0.5°C. Based on the method described by Kline and McClintock,[32] the uncertainty of the Nusselt number ratio is about 6% for the high Reynolds number. For the low Reynolds number ($Re = 5 \times 10^3$), where more heat loss occurs and the uncertainty of the individual measurements increases, the maximum uncertainty is about 17% on the leading wall in the first pass under rotating conditions. The maximum uncertainty of the friction factor ratio is 7% at $Re = 10 \times 10^3$. The uncertainty of the friction factor ratio decreases to approximately 3% at the highest Reynolds number.

Results and Discussion

Rib Configurations and Secondary Flow Patterns

Figure 5 shows the rib configurations and conceptual secondary flow patterns induced by rotation and ribs. All of the ribs have an angle of 45 deg to the mainstream flow and are placed parallel on the leading and the trailing walls, except the crossed V-shaped ribs. The secondary flow patterns for angled ribs and V-shaped ribs have been verified by the numerical prediction of Al-Qahtani et al.[33] and Su et al.,[34] respectively.

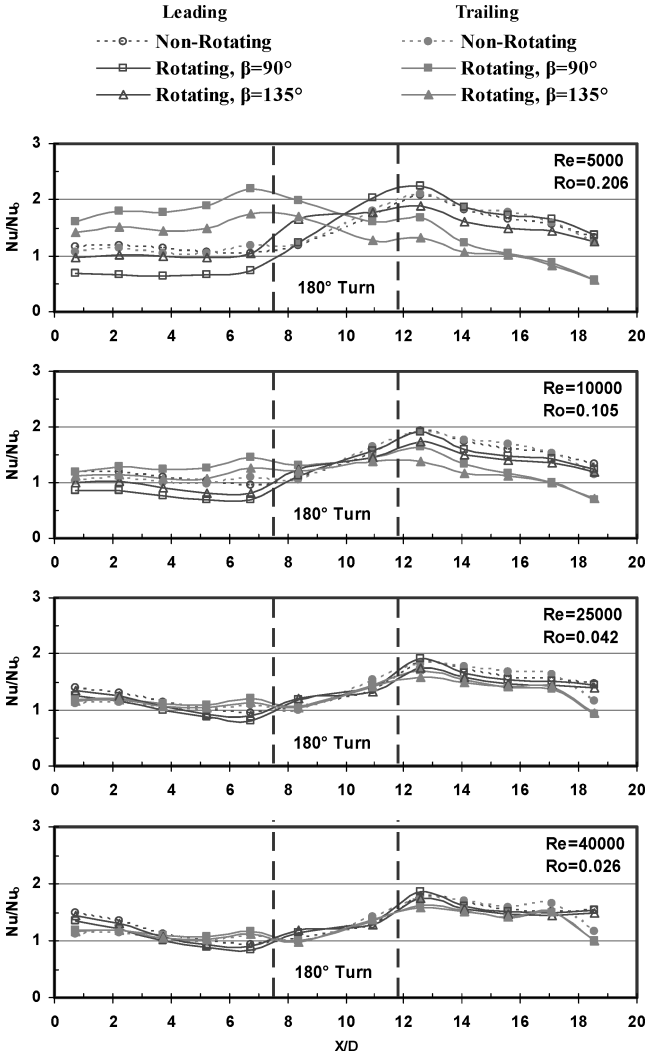

Fig. 6 Nusselt number ratio distributions for case a): smooth channel.

Azad et al.[23] gave detailed descriptions of the secondary flow patterns in a 2:1 rotating duct with smooth and 45-deg angled ribs. Figure 5a (smooth wall) shows the secondary flow induced by rotation only. As mentioned by Azad et al.,[23] these counter-rotating vortices are generated by the Coriolis force. In the first pass, the flow moves in the radial outward direction, and the Coriolis force directs the coolant from the core toward the trailing wall. In the second pass, the flow moves in the radial inward direction and the Coriolis force directs the coolant to the leading wall. For a channel orientation of 90 deg these vortices are symmetrical and directly act either on the trailing (first pass) or the leading (second pass) walls. When the channel orientation changes to 135 deg, these vortices are asymmetric and migrate diagonally away from the corner region between the inner and leading walls toward the center in the first pass, and from the corner region between the inner and trailing walls toward the center in the second pass.

Figure 5b shows the 45-deg angled ribs induced secondary flow pattern. The parallel 45-deg angled ribs create symmetric counter-rotating vortices parallel to the ribs. These vortices enhance heat transfer on both the leading and trailing walls compared to the smooth wall case. When the ribbed channel is rotating, the rotation-induced vortices interacted with the rib-induced vortices. The result of this interaction is to increase heat transfer on the first-pass trailing and second-pass leading walls, while decreasing heat transfer on the first-pass leading and second-pass trailing walls. The V-shaped ribs create two pairs of counter-rotating vortices as shown in Fig. 5c. The vortices move parallel to the ribs from the center of the channel to either the inner or outer walls. As shown in the literature, the V-shaped ribs have higher heat transfer enhancement than the 45-deg angled ribs in the nonrotating case because the vortices create more mixing in the center of the channel. For the rotating case, the Coriolis-force-induced vortices (as shown in the smooth channel) interact with the rib-induced vortices. The rotating direction of the Coriolis-force-induced vortices is parallel to the rib-induced vortices on the first-pass trailing and second-pass leading wall, but against the rib-induced vortices on the first-pass leading and second-pass trailing walls. It can be expected that rotation enhances heat transfer on the first-pass trailing and second-pass leading walls and reduces heat transfer on the first-pass leading and second-pass trailing walls.

The discrete 45-deg angled ribs are shown in Fig. 5d. This rib arrangement is created by breaking the 45-deg angled ribs in the center and then shifting one side of the ribs by half of the rib pitch. Instead of one pair of counter-rotating vortices, the discrete 45-deg angled ribs create two pairs of counter-rotating vortices parallel to the rib direction in each pass. The discrete angled ribs are expected to create more mixing in the core of the channel and, therefore, enhance the heat transfer more than the 45-deg angled ribs. With rotation, the Coriolis-force-induced vortices will act against one of the rib-induced vortices on either the leading or the trailing wall, but parallel to the other on the opposite wall (trailing or leading wall) in each pass. The discrete V-shaped ribs are also created by breaking the V-shaped ribs in the center and shifting one side of the rib by half of the rib pitch. However, it creates the same number of vortices as the V-shaped ribs do. The secondary flow patterns are similar to the V-shaped ribs.

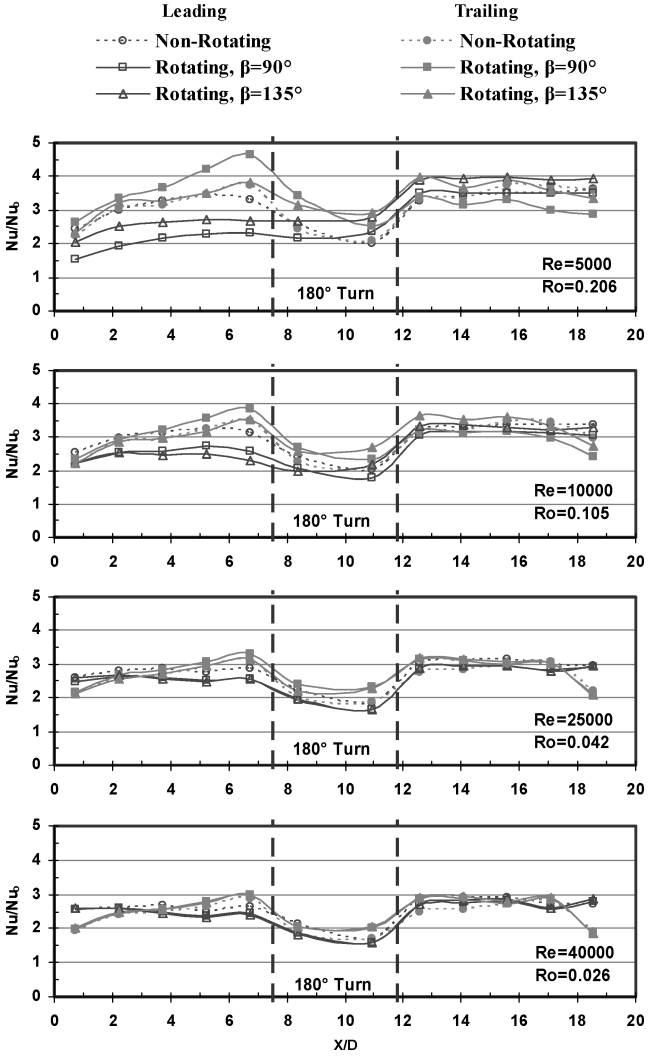

Fig. 7 Nusselt number ratio distributions for case b): 45-deg angled ribs.

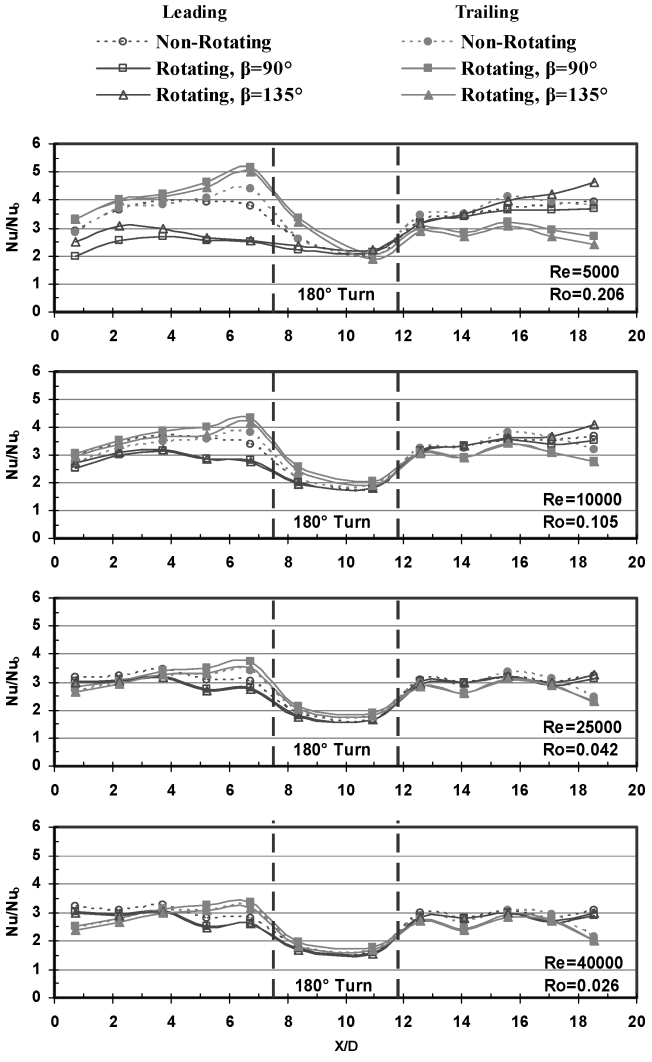

Fig. 8 Nusselt number ratio distributions for case c): V-shaped ribs.

Figure 5f shows the crossed V-shaped ribs. This crossed V-shaped rib and the V-shaped ribs are identical on the first-pass trailing and second-pass leading walls, but have opposite rib directions on the first-pass leading and second-pass trailing walls. As shown in Fig. 5f, the crossed V-shaped ribs create a pair of large counter-rotating vortices that trap the colder coolant inside the vortices. Therefore, less heat transfer can be expected for the nonrotating case due to the smaller temperature gradient near the walls. When the channel rotates, the Coriolis-force-induced vortices and the rib-induced vortices rotate in the same directions. These vortices become stronger and were expected to change the heat transfer in the rotating channel.

Regionally Averaged Heat Transfer Distributions

The regionally averaged heat transfer (Nusselt number ratio) distributions for each case are shown in Figs. 6 to 11. Each figure contains the nonrotating and rotating ($\beta = 90$ and 135 deg) results at four Reynolds numbers. For the smooth channel (Fig. 6), the nonrotating heat transfer distributions show a smooth decreasing trend in the first pass. It reaches the fully developed value before the turn. Through the 180-deg turn, the heat transfer is enhanced due to the direction change of the flow, which causes high turbulence inside this region. After the turn, the heat transfer is enhanced because of the strong turn effect. In the remainder of the second pass, the heat transfer decreases as the flow develops. For the rotating case, the rotation effect increases heat transfer on the trailing wall and decreases heat transfer on the leading wall in the first pass. However, both the trailing and leading walls have lower heat transfer in the second pass when compared to the nonrotating case. The difference of heat transfer between leading wall and trailing wall is smaller in the second pass than in the first pass. It is believed that the 180-deg sharp turn has a greater effect on the heat transfer enhancement than rotation in the second pass. As the Reynolds number increases (rotation number decreases), the rotation effect is reduced; in other words, the difference between the Nusselt number ratios on the leading and trailing surfaces decreases. When the channel is positioned at an angle of 135-deg, the rotation-induced secondary flow vortices are asymmetric, as shown in Fig. 5a. As expected, the 135-deg channel orientation has a smaller rotation effect than the 90-deg channel orientation. For all rotating and nonrotating cases, the Nusselt number ratio decreases as the Reynolds number increases.

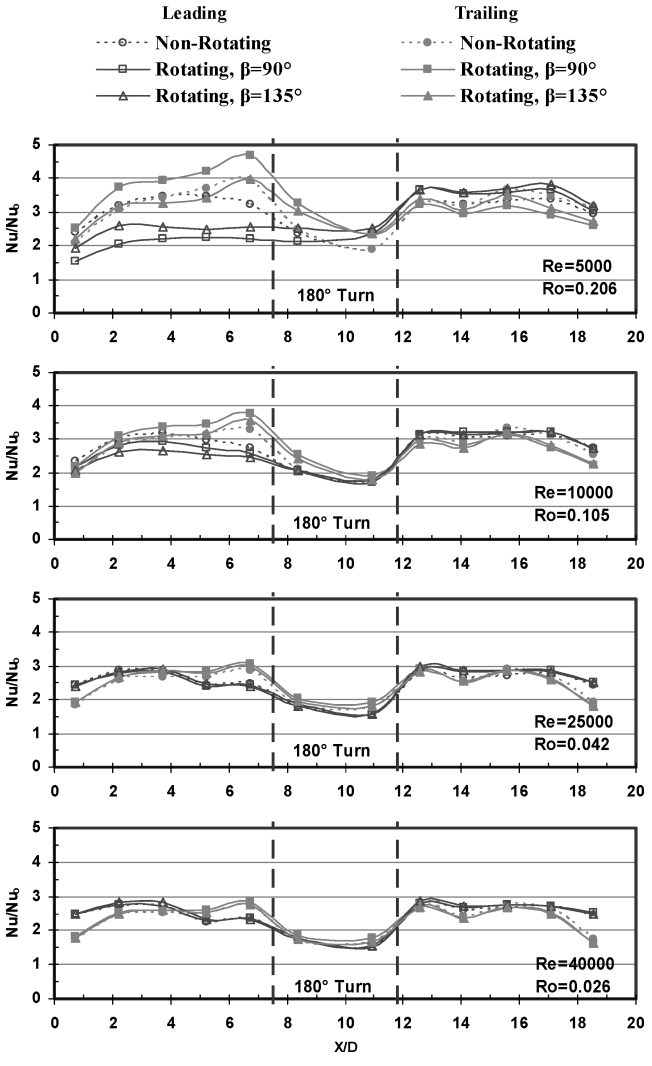

Fig. 9 Nusselt number ratio distributions for case d): discrete 45-deg angled ribs.

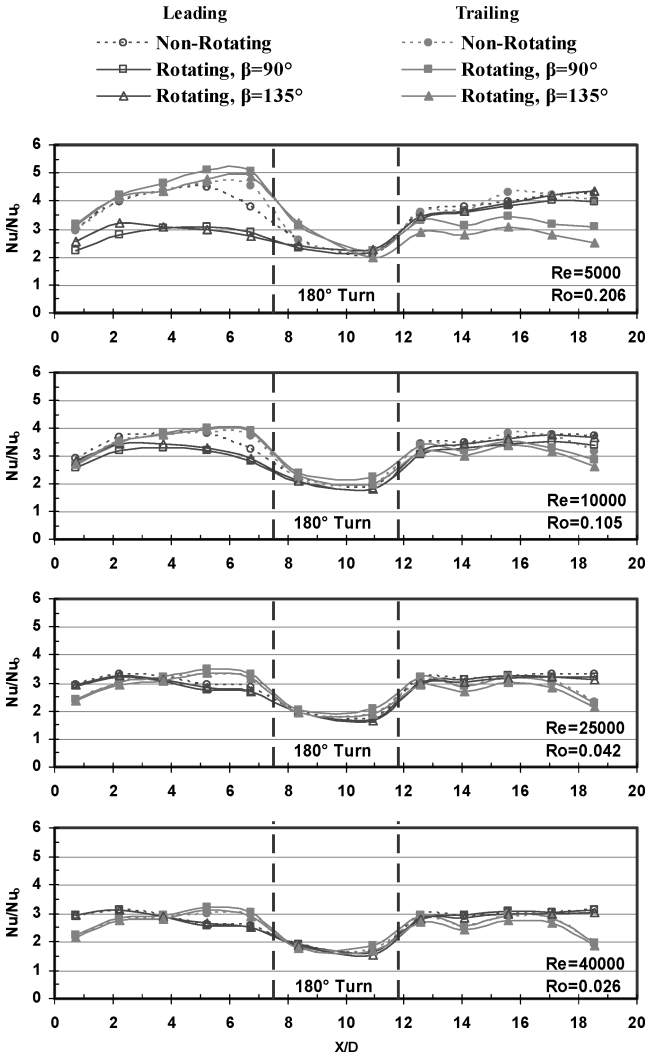

Fig. 10 Nusselt number ratio distributions for case e): discrete V-shaped ribs.

The results for 45-deg angled ribs are shown in Fig. 7. For the nonrotating case, the 45-deg angled ribs enhance heat transfer about three times more than the smooth wall. The turn region has a lower enhancement because of fewer ribs in this region. In the second pass, the enhancement is different to the smooth wall case, which has greater enhancement in the second pass. In the smooth channel, the turn significantly enhances heat transfer in the second pass. In the ribbed channel, the turn effect disturbs the rib-induced vortices. Therefore, the second pass has slightly lower heat transfer enhancement than the first pass.

Similarly to the smooth case, the Coriolis force enhanced heat transfer on the trailing wall and reduced heat transfer on the leading wall in the first pass under rotation. In the second pass, the Coriolis force acts in the opposite direction; the leading wall heat transfer is enhanced, and the trailing wall is reduced. Again, the heat transfer

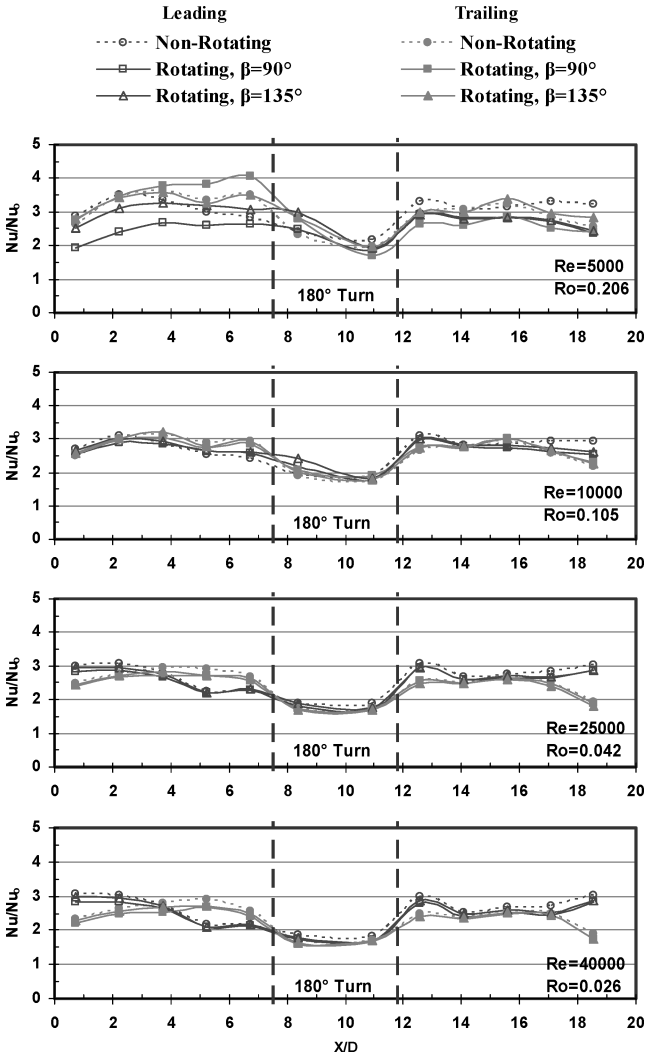

Fig. 11 Nusselt number ratio distributions for case f): crossed V-shaped ribs.

difference between the leading wall and the trailing wall is smaller in the second pass due to the turn effect. When the channel is oriented at 135 deg, the rotation-induced vortices impinge on the corner of the outer wall and trailing wall. It is expected to have a smaller rotation effect than for the channel oriented at 90 deg.

Figure 8 shows the results for the V-shaped ribs. The nonrotating heat transfer distribution has a trend similar to that of the 45-deg angled ribs, but the heat transfer enhancement is higher than for the 45-deg angled ribs. This confirms the previous studies that the V-shaped ribs perform better than the angled ribs in nonrotating channels. The rotation effect slightly increases the heat transfer on the first-pass trailing wall and the second-pass leading wall. However, it significantly decreases the heat transfer on the first-pass leading wall and the second-pass trailing wall. Again, the first pass has a greater heat transfer difference between the leading and trailing walls than the second pass. The effect of channel orientation on heat transfer is smaller in V-shaped ribs when compared to the smooth channel and the 45-deg angled ribs.

Figure 9 shows the heat transfer results for the discrete 45-deg angled ribs. The results show a distribution similar to that for the 45-deg angled ribs. The ribbed walls enhance heat transfer about three times more than the smooth wall in the first pass and second pass. Less heat transfer enhancement is observed in the turn region than with the previous rib cases. The difference between discrete angled ribs and nondiscrete ribs is that the discrete ribs are broken in the center of channel. Therefore, the discrete ribs may induce two pairs of vortices, and the heat transfer will be enhanced. However, the heat transfer distributions did not show a significant difference when compared to the nondiscrete angled ribs. Another possibility is that the discrete ribs still induced one pair of vortices, but the vortices were shifted to the next rib in the center of the channel. In this case, the discrete angled ribs may have heat transfer enhancement similar to that for the nondiscrete angled ribs. Similarly to the nondiscrete angled ribs, the Coriolis force creates more heat transfer in the first pass than in the second pass.

The regional heat transfer distributions for the discrete V-shaped ribs are shown in Fig. 10. Again, the results are very similar to those for the V-shaped ribs. The enhancement is about the same as the V-shaped ribs, but is higher than the angled ribs and the discrete angled ribs for the nonrotating case. With rotation, the Coriolis force creates a significant heat transfer difference between the leading and the trailing walls in the first pass. However, the difference is reduced in the second pass due to the strong turn effect, as seen in the previous results. The channel orientation effect is smaller with the V-shaped ribs and discrete V-shaped ribs than with the angled ribs and discrete angled ribs.

Figure 11 shows the crossed V-shaped ribs regional heat transfer distributions. As seen in Fig. 5f, this rib configuration is similar to V-shaped ribs, but has opposite V directions on the leading wall in the first pass and the trailing wall in the second pass. The result shows a similar trend to the V-shaped ribs but with less enhancement in heat transfer for all conditions. In addition, the heat transfer difference between the leading wall and the trailing wall due to rotation is reduced in this rib configuration. The crossed V-shaped ribs create one pair of rib-induced vortices that has greater strength than for the V-shaped ribs. However, the larger vortices circulate along the walls. The cold flow is trapped inside the vortices. As a result, the enhancement is smaller compared to V-shaped ribs, which have better mixing in the center of the duct. With rotation, the Coriolis force further strengthens these vortices, which reduces the difference of enhancement between the leading wall and the trailing wall. On the other hand, the V-shaped ribs still have two pairs of vortices induced by rotation. The rotation may further strengthen the vortices on the trailing wall in the first pass and on the leading wall in the second pass. Therefore, the heat transfer difference is greater than the crossed V-shaped ribs.

Channel-Averaged Nusselt Number Ratio for Nonrotating Cases

The channel-averaged Nusselt number ratios for the nonrotating cases are shown in Fig. 12. The channel averaged values exclude the turn region. The first-pass-averaged value includes data points on both the leading and trailing walls from $X/D = 0.75$ to 6.75. The second-pass-averaged values include data points on both the leading and trailing walls from $X/D = 12.56$ to 18.56. For nonrotating cases, the heat transfer enhancement is primarily due to the rib-induced secondary flows: mainstream flow reattachment and secondary flow developed along the rib direction (Han et al.[1]). When the mainstream flow passes the ribs, a flow separation occurs on the top of the ribs and then the flow reattaches on the wall between ribs. This flow reattachment will significantly enhance heat transfer. As the flow approaches the ribs, the ribs will guide the near-wall coolant to move along the ribs. The rib-induced vortices are shown in Fig. 5. When the coolant moves along the ribs, it picks up heat from the wall and the boundary layer becomes thicker. Therefore, the heat transfer enhancement is reduced along the ribs direction.

The V-shaped ribs are shorter than the angled ribs. The boundary layer redevelops along each side of the ribs, resulting in a thinner boundary layer. As expected, the results show that the V-shaped ribs and the discrete V-shaped ribs have higher heat transfer enhancement than the 45-deg angled ribs and the discrete 45-deg angled ribs in both passes. For low Reynolds number, the discrete ribs have better heat transfer than the nondiscrete ribs in the first pass for both angled ribs and V-shaped ribs. At high Reynolds number, the nondiscrete ribs have better heat transfer enhancement than the discrete ribs in the first pass. However, in the second pass, the discrete V-shaped ribs perform better heat transfer than the V-shaped ribs and the 45-deg angled ribs are better than the discrete 45-deg angled ribs for the entire range of Reynolds number. The crossed V-shaped ribs

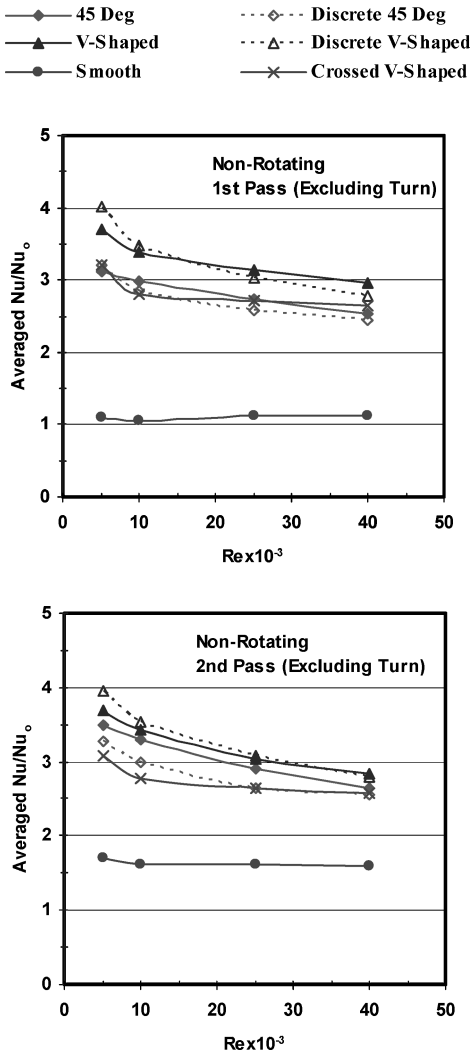

Fig. 12 Channel-averaged Nusselt number ratios for nonrotating cases.

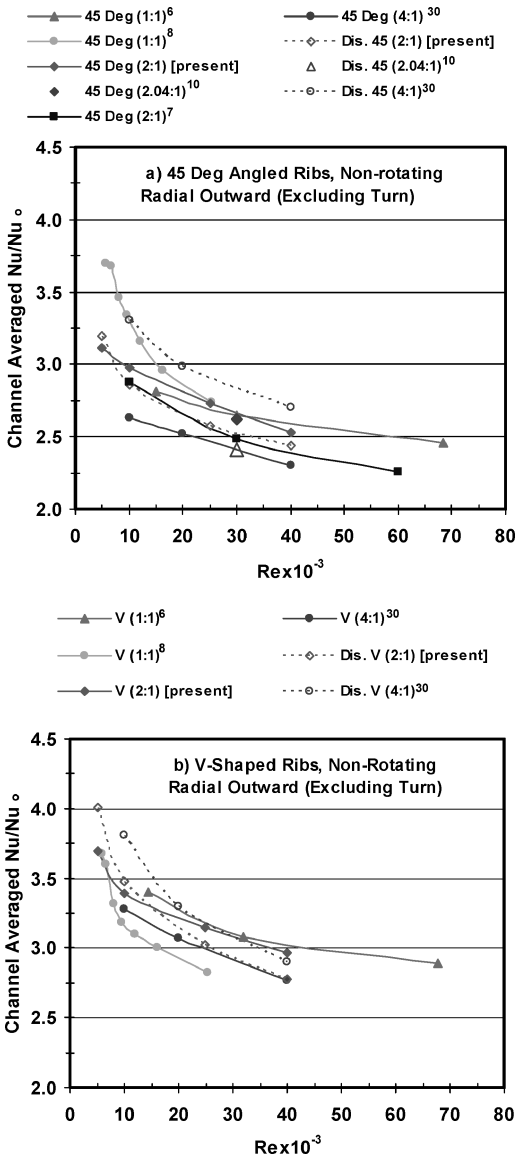

Fig. 13 Comparison of channel averaged Nusselt number ratios for nonrotating cases.

have the worst heat transfer enhancement in both passes. As the Reynolds number increases the Nusselt number ratios decrease for all rib configurations. The ribbed channels enhance heat transfer about three times more than the smooth channel in the first pass, but only about two times more in the second pass for the best case (discrete V-shaped ribs). That is because the 180-deg sharp turn already created approximately 50% more enhancement in the second pass than the first pass in a smooth channel.

Comparison with Previous Studies

Figure 13 shows the comparison of 45-deg angled ribs and V-shaped ribs with previous studies in the first-pass radial outward flow under nonrotating condition. The present channel-averaged values exclude the turn region. The dimensions for each study are listed in Table 1. From Fig. 13a, the heat transfer enhancement follows the order of channel aspect ratio. The higher-aspect-ratio channel (4:1) has the lowest enhancement. The aspect ratio 1:1 (Taslim et al.[8] and Han et al.[6]) ducts have the highest enhancement, followed by aspect ratio 2:1 (Park et al.,[7] Cho et al.,[10] and present) and aspect ratio 4×1 (Wright et al.[30]) for the 45-deg angled ribs. As discussed in the previous section, the heat transfer enhancement is primarily due to flow reattachment and rib-induced vortices. Also, the enhancement decreases along the ribs due to boundary layer development. For the same e/D ratio, the higher-aspect-ratio channel has longer ribs. Therefore, the enhancement is reduced because of the longer rib. For the same aspect ratio, the higher e/D ratio represents a higher blockage ratio, which gives better heat transfer enhancement (Taslim et al.[8]), because the higher blockage ratio will create more flow acceleration when flow passes the ribs.

Discrete 45-deg angled ribs are also compared in Fig. 13a. Cho et al.[10] and the present results show the discrete 45-deg angled ribs have less enhancement than the 45-deg angled ribs. Both have an aspect ratio of about 2:1. However, Wright et al.[30] show a different trend for an aspect ratio of 4:1.

V-shaped ribs and discrete V-shaped ribs are compared with previous studies in Fig. 13b. Again the comparison is limited to nonrotating and radial outward flow. Similar to Fig. 14a, the lower-aspect-ratio channel has higher enhancement for V-shaped ribs except for the result from Taslim et al.[8] The present results show the discrete V-shaped ribs have a higher enhancement at low Reynolds number. The trend reverses at Reynolds number higher than 15×10^3. However, Wright et al.[30] show higher enhancement for discrete V-shaped rib for all Reynolds numbers in a 4:1 channel.

The previous study by Wright et al.[30] and the present study have the same channel height and rib height. However, the present study has a smaller hydraulic diameter. For the same Reynolds number, the present study has greater flow velocity. The increased flow velocity creates a greater flow reattachment effect in the nondiscrete rib channel due to the high momentum. As seen in Fig. 13, the low-aspect-ratio ducts have higher heat transfer enhancement. For discrete ribs, there is a gap between the ribs that create a flow path

Table 1 Dimensions of various studies

Study	AR	W, mm	H, mm	D, mm	Rib	e/D	e/H	P/e	$\Delta\rho/\rho$
Han et al.[6]	1:1	50.8	50.8	50.8	45, V	0.0625	0.0625	10	
Taslim et al.[8a]	1:1	76.2	76.2	76.2	45, V	0.0833	0.0833	10	
Park et al.[7]	2:1	102	51	68	45, V	0.047	0.0627	10	
Cho et al.[10b]	2.04:1	102	50	67.3	45	0.0743	0.1	10	
Present[b]	2:1	25.4	12.7	16.93	45, V	0.0938	0.125	10	0.115
Wright et al.[30b]	4:1	50.8	12.7	20.32	45, V	0.0781	0.125	10	0.12

[a]Staggered ribs. [b]Included discrete and nondiscrete ribs.

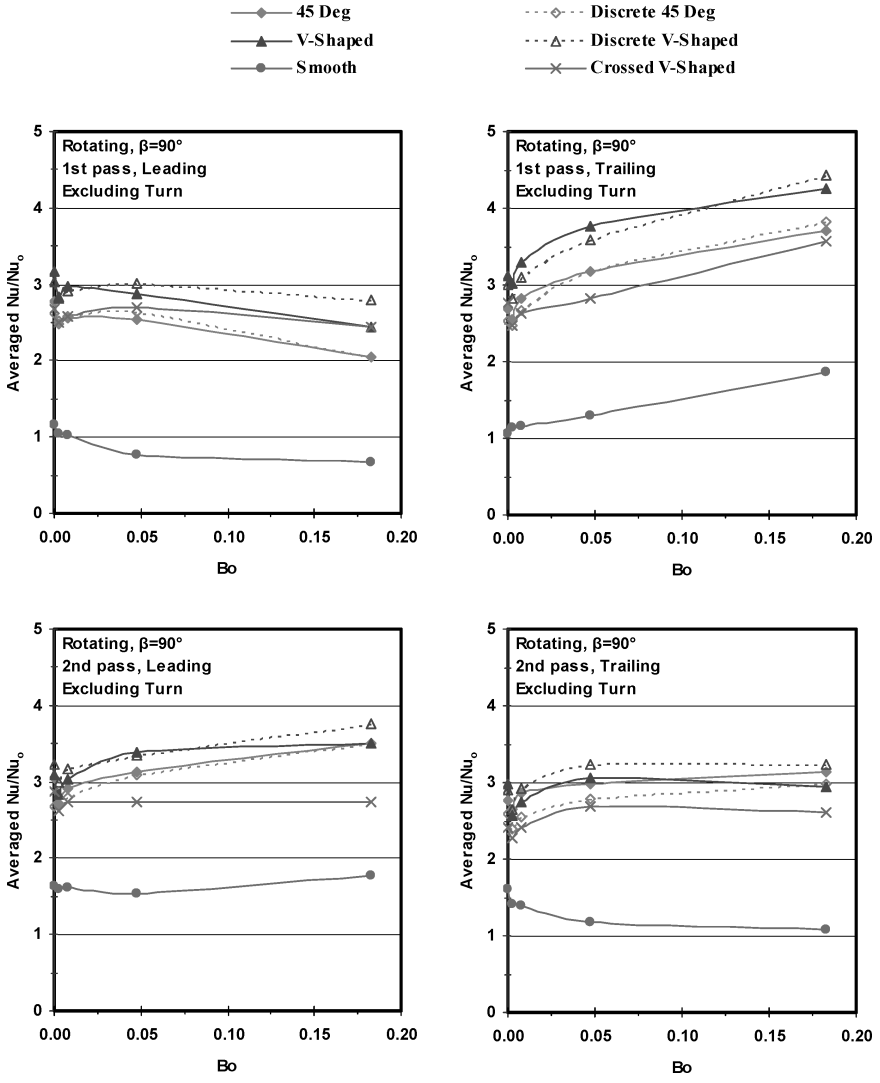

Fig. 14 Channel-averaged Nusselt number ratios for rotating cases (β = 90 deg).

for the coolant. Part of the coolant will move through the gap instead of passing over the ribs. This will reduce the flow reattachment effect. This effect is more significant in the 2:1 duct because of the increased velocity. On the other hand, the 4:1 duct has longer ribs than the 2:1 duct. As discussed in the previous section, the heat transfer enhancement reduced along the rib direction. The downstream of the half ribs in the 4:1 duct has the lowest heat transfer. When the ribs are broken into two pieces, the boundary layer redevelops on the second half of the ribs; with a thinner boundary layer, there is more heat transfer enhancement. This effect is greater in the 4:1 duct with longer ribs. Therefore, the discrete and nondiscrete perform differently in the 2:1 duct and the 4:1 duct.

Rotation Effect on Channel Averaged Nusselt Number Ratio

The effect of rotation on heat transfer enhancement is shown in Fig. 14 for the channel orientation of 90 deg and Fig. 15 for the channel orientation of 135 deg. The averaged value excludes the turn region. The first-pass averaged values include data points from $X/D = 0.75$ to 6.75. The second-pass averaged value includes data points from $X/D = 12.56$ to 18.56. Instead of using rotation number, the buoyancy parameter is used to present the combined effects of rotation and buoyancy forces. These two parameters are defined below by Wagner et al.,[11]

$$Ro = \Omega D/V \tag{6}$$

$$Bo = (\Delta\rho/\rho)(Ro)^2(R/D) \tag{7}$$

The Coriolis force due to rotation creates a pair of counter-rotating vortices that impinge on the trailing wall for radial outward flow (first pass) and on the leading wall for radial inward flow (second pass). As a result, these two walls experience heat transfer enhancement due to rotation. The opposite walls (leading wall in the first pass and trailing wall in the second pass) experience reduced heat transfer.

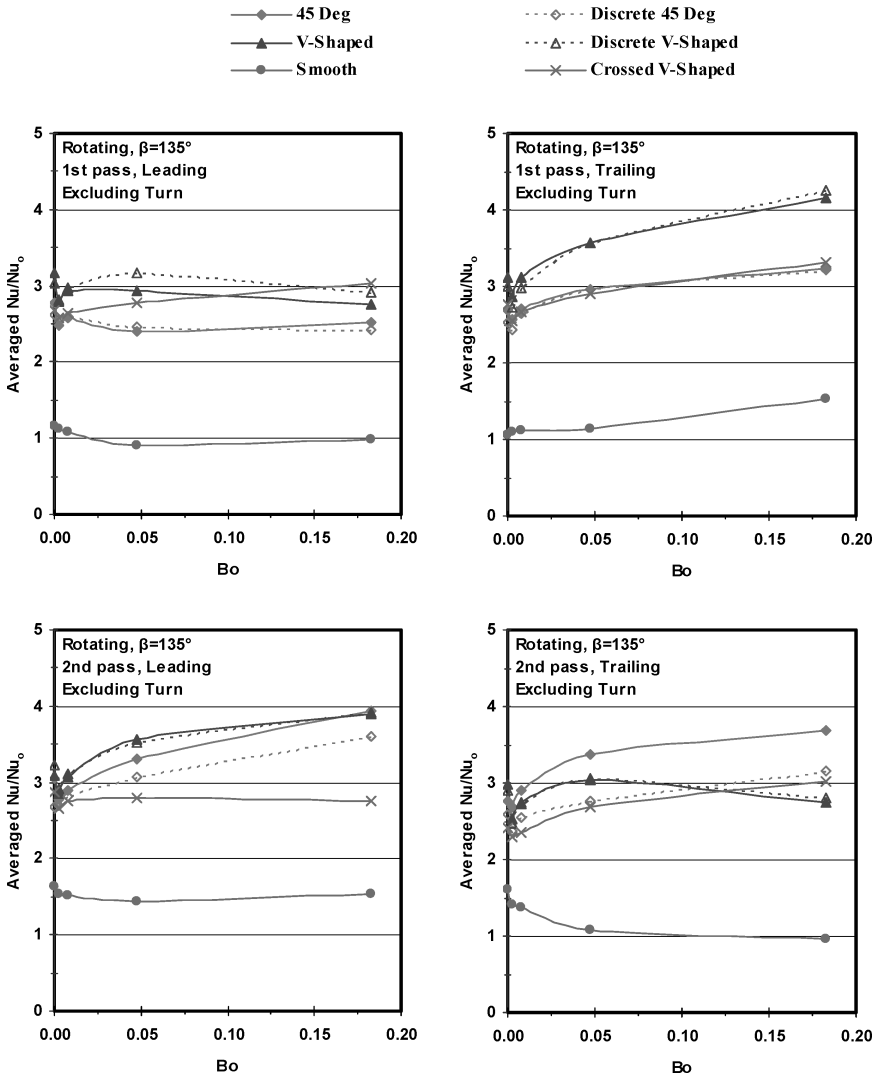

Fig. 15 Channel-averaged Nusselt number ratios for rotating cases (β = 135 deg).

The smooth wall results represent the rotation effect only, as seen in Fig. 14. The rib walls have a trend similar to that for the smooth walls, but with much greater enhancement.

As expected, the V-shaped ribs and discrete V-shaped ribs have higher enhancement than the 45-deg angled ribs and the discrete 45-deg angled ribs. As expected, the crossed V-shaped ribs poorly; in fact, the crossed V-shaped ribs yielded the smallest enhancement in most cases. The V-shaped ribs and the discrete V-shaped ribs have two pairs of vortices in each pass, as shown in Fig. 5. These small vortices interact in the core zone of the channel and create more mixing. The vortices then bring cold coolant from the core zone to the walls. Therefore, the V-shaped ribs and the discrete V-shaped ribs have the highest enhancement. The crossed V-shaped ribs create one pair of vortices that trap cold coolant as seen in Fig. 5f. As a result, the enhancement is less than for the other rib arrangements as discussed previously. With rotation, the Coriolis-force-induced vortices have the same rotating directions as the crossed induced vortices. Therefore, these vortices are further strengthened by the rotation and they are stronger than the vortices that are seen in the other ribbed channels. However, the cold coolant is still trapped inside the core of the vortices, which cause less enhancement, than for the other ribbed channels for rotating cases. The stronger and warmer vortices reduce the heat transfer difference between the leading wall and the trailing wall.

The angled ribs create one pair of counter-rotating vortices that move along the ribs from the inner wall to the outer wall in the first pass and from the outer wall to the inner wall in the second pass. When the channel is rotating, the Coriolis-force-induced vortices impinge on the first-pass trailing wall. Then they separate and move in two directions: one to the inner wall, the other to the outer wall. After traveling on the inner and the outer walls, these two secondary flows merge at the center of the leading wall in the first pass, as shown in Fig. 5b. The rotation-induced vortices interact with the rib-induced vortices in the center of the channel. However, the enhancements are lower than the V-shaped ribs. That is due to the longer ribs creating a thicker boundary layer when the coolant moves along the rib.

Overall, for the rotating case of a 90-deg channel orientation, the discrete V-shaped ribs perform better than the V-shaped ribs, especially for high Reynolds number. The discrete 45-deg angled ribs and 45-deg angled ribs have about the same heat transfer enhancement except on the second-pass trailing wall. On the second-pass trailing wall, the 45-deg angled ribs have better enhancement than the discrete 45-deg angled ribs. The crossed V-shaped ribs have the lowest enhancement in most cases.

Channel-averaged Nusselt number ratios for the channel oriented at 135 deg are shown in Fig. 15. Under this channel orientation, the rotation-induced vortices impinge on the corner of the trailing outer wall in the first pass and on the corner of the leading outer wall in the second pass. Therefore, the effect of rotation is expected to be reduced. The results are similar those of to the 90-deg channel orientation. Due to the reduced rotation effect, the enhancements in the first pass are higher on the leading and lower on the trailing wall when compared to the 90-deg channel orientation case. In the first

pass, the V-shaped ribs and the discrete V-shaped ribs have higher enhancements than the 45-deg angled ribs and the discrete 45-deg angled ribs. The discrete and nondiscrete ribs have about the same enhancement for both 45-deg angled ribs and V-shaped ribs, except on the leading wall. The discrete V-shaped ribs are better than the V-shaped ribs on the leading wall. The crossed V-shaped ribs have less difference between the leading wall and the trailing wall in the first pass. In the second pass, the heat transfer difference between the leading and the trailing walls is less than in the first pass due to a strong turn effect, as discussed previously. Therefore, the trends are different from the first pass when the channel is orientated at 135 deg.

In the second pass, the leading wall experiences enhancement because of the rotation effect. As the buoyancy parameter increases (rotation effect increases), the enhancement increases for all ribbed walls, except the crossed V-shaped ribs. On the trailing wall, reduced enhancement is expected. However, the 45-deg angled ribs, the discrete 45-deg angled ribs, and the crossed V-shaped ribs show an increasing trend as the buoyancy parameter increases.

For the 45-deg angled ribs and discrete 45-deg angled ribs with channel orientation 135 deg, the rotation-induced vortices and the rib-induced vortices move in the same directions (Fig. 5) in the second pass. The rotation-induced vortices strengthen the rib-induced vortices at the beginning of the angled ribs. Therefore, the rotation effect increases heat transfer on both the leading and the trailing walls. For the nondiscrete angled rib, these vortices keep moving to the end of ribs, which enhances heat transfer more than the discrete angled rib. In addition, this enhancement is greater than in the first pass. As the buoyancy parameter increasing, this effect becomes

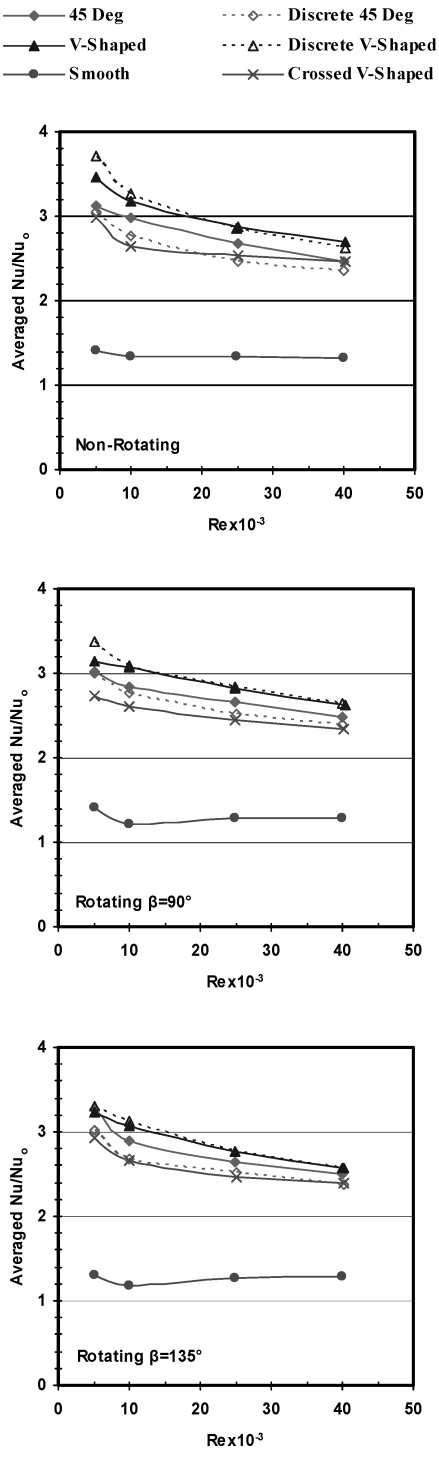

Fig. 16 Overall channel-averaged Nusselt number ratios.

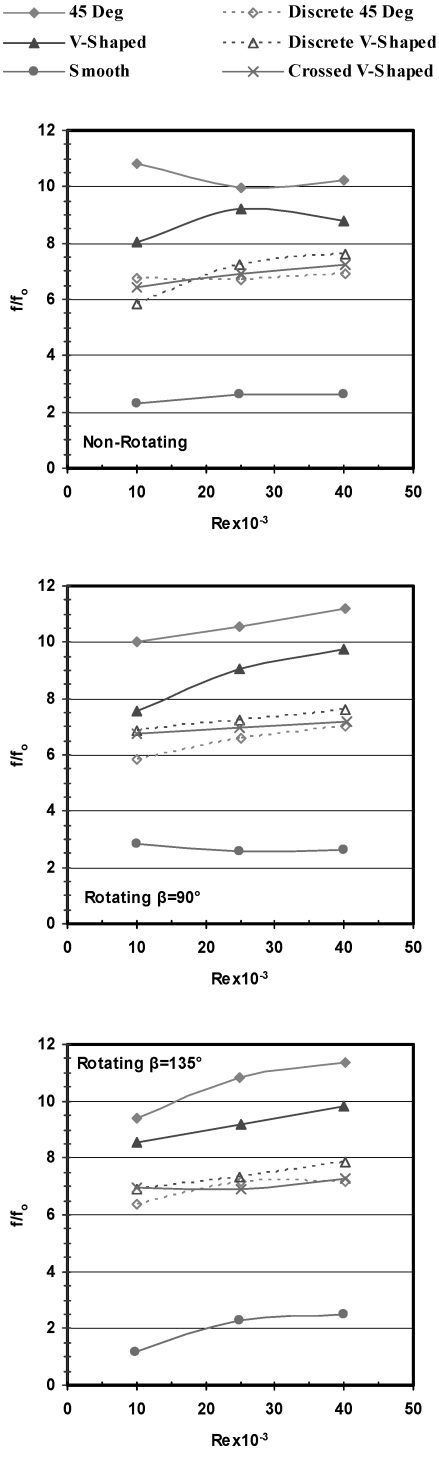

Fig. 17 Overall friction-factor ratios.

greater. An expected decreasing trend is seen for V-shaped ribs and discrete V-shaped ribs on the trailing wall.

Overall Friction Factor and Thermal Performance

For turbine blade designers, it is necessary to evaluate the increased pumping power against the overall heat transfer enhancement for each rib arrangement. This information can be obtained by calculating the overall thermal performance of each rib arrangement. To calculate the overall thermal performance of each rib arrangement, the overall heat transfer and pressure loss are required. The overall channel-averaged Nusselt ratio is obtained by averaging the leading and trailing surfaces of every point (included the turn). As shown in Fig. 16, the channel-averaged Nusselt number ratio of the smooth nonrotating channel is above one. This is due to the heat transfer enhancement at the entrance and the 180-deg sharp turn. The results show that the V-shaped and discrete V-shaped ribs yield the greatest heat transfer enhancement for the nonrotating case. For rotating cases ($\beta = 90$ and 135 deg), the heat transfer trends are similar to those in the nonrotating case.

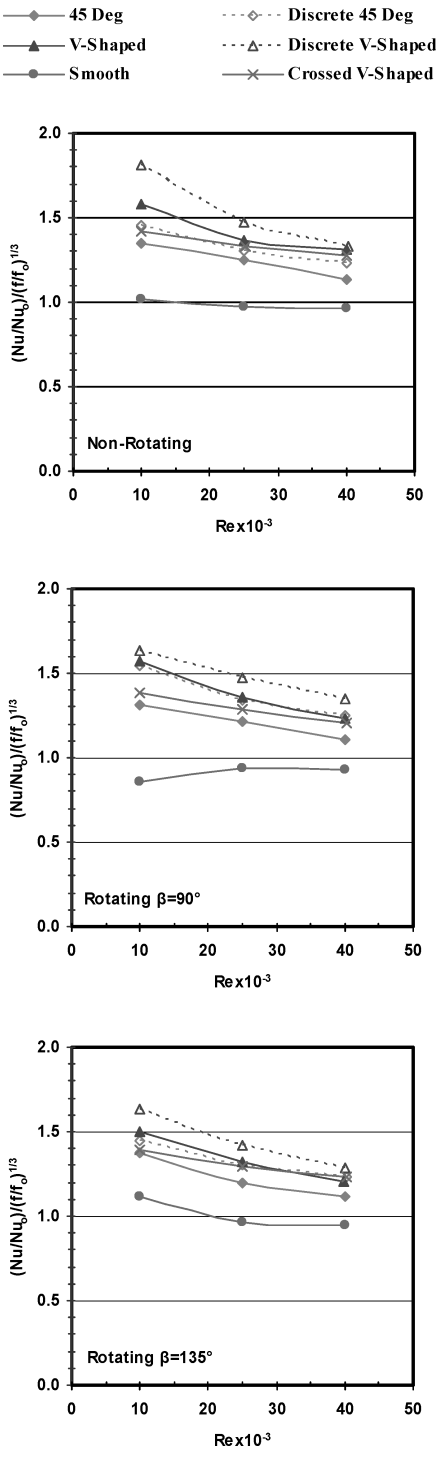

Fig. 18 Overall thermal performances.

The increased pumping power can be expressed by the friction factor. Figure 17 shows the overall friction factor ratio for each rib arrangement. The pressure penalty for smooth channels is between 2 to 3. The friction factors are elevated above unity due to the pressure loss incurred in the 180-deg sharp turn. As shown in Fig. 17, the 45-deg angled ribs have the highest friction-factor ratio for both rotating and nonrotating cases, followed by the V-shaped ribs. The levels of the friction-factor ratios are about the same for the discrete 45-deg angled ribs, discrete V-shaped ribs, and crossed V-shaped ribs. The trends are similar for nonrotating and rotating cases.

The overall thermal performance (Fig. 18) is calculated using Eq. (5). Both overall channel-averaged Nusselt number ratio and overall friction-factor ratio are used. The performance of the smooth channel is approximately one for rotating and nonrotating cases. The discrete V-shaped ribs have the highest thermal performance. The heat transfer is about the same; however, the pressure loss is much less. The 45-deg angled ribs have the poorest thermal performance among those ribbed channels because of their high pressure loss.

Conclusions

This study provided heat transfer and pressure loss measurements on discrete and nondiscrete ribs for 45-deg angled and V-shaped rib arrangements in a two-pass rotating channel with an aspect ratio of 2:1. The measurements are taken at Reynolds numbers of 5, 10, 25, and 40×10^3 for each case. At a fixed rotating speed of 550 rpm, the corresponding rotation numbers are 0.206, 0.105, 0.042, and 0.026. From the present study, the main conclusions are as follows:

1) The V-shaped ribs and the discrete V-shaped ribs have better heat transfer enhancements than the 45-deg angled ribs and the discrete 45-deg angled ribs for nonrotating and most rotating cases. The crossed V-shaped ribs have the worst heat transfer enhancement except on the rotating leading wall in the first pass for both channel orientations.

2) For nonrotating cases, the present results ($AR = 2{:}1$) show that the discrete V-shaped ribs have higher heat transfer enhancements than the nondiscrete V-shaped ribs at lower Reynolds number. At higher Reynolds number, the nondiscrete V-shaped ribs have better heat transfer than the discrete V-shaped ribs, especially in the first pass. The nondiscrete 45-deg angled ribs have better enhancement than the discrete 45-deg angled ribs in both passes. However, the previous study by Wright et al.[30] showed different results. Their discrete-type ribs have higher enhancement than the nondiscrete-type ribs in a single-pass 4:1 duct. The result may be due to the channel-aspect-ratio effect.

3) For the rotating case with a channel orientation of 90 deg, the discrete-type ribs and the nondiscrete-type of ribs have about the same heat transfer enhancement. The exceptions are that the discrete V-shaped ribs have higher enhancement than the nondiscrete V-shaped ribs on the first-pass leading wall and the second-pass trailing wall, and the nondiscrete 45-deg angled ribs have better enhancement than discrete 45-deg angled ribs on the second-pass trailing wall.

4) For the rotating case with a channel orientation of 135 deg, the discrete V-shaped ribs and the nondiscrete ribs have about the same heat transfer enhancement, except that the discrete V-shaped ribs have higher enhancement than the nondiscrete V-shaped ribs on the first-pass leading wall. The nondiscrete 45-deg angled ribs and discrete 45-deg angled ribs have the same enhancement in the first pass, but the nondiscrete 45-deg angled ribs have higher enhancement in the second pass than the discrete 45-deg angled ribs.

5) The rotation effect is greater on heat transfer in the first pass than in the second pass due to the turn effect. The crossed V-shaped rib has less heat transfer difference between the leading and trailing walls under rotating conditions because the ribs create one pair of large and stronger vortices.

6) For the rotating case at 135-deg channel orientation, the 45-deg angled ribs, the discrete 45-deg angled ribs, and the crossed V-shaped ribs have an increasing trend on the trailing wall as the buoyancy parameter increases. This is due to the rotation-induced vortices moving in the same direction as the rib-induced vortices.

7) The discrete V-shaped ribs have the best overall thermal performance for all cases due to their high heat transfer coefficient and low pressure loss. The 45-deg angled ribs have the highest pressure loss for rotating and nonrotating cases. Therefore, they are the worst rib arrangement in the present study.

Acknowledgments

This publication was prepared with the support of the US Department of Energy, Office of Fossil Energy, National Energy Technology Laboratory. However, any opinions, findings, conclusions, or recommendations expressed herein are those of the authors and do not necessarily reflect the views of the DOE.

References

[1]Han, J. C., Dutta, S., and Ekkad, S. V., *Gas Turbine Heat Transfer and Cooling Technology*, Taylor and Francis, New York, 2000.

[2]Metzger, D. E., and Sahm, M. K., "Heat Transfer around Sharp 180° Turns in Smooth Rectangular Channels," *Journal of Heat Transfer*, Vol. 108, 1986, pp. 500–506.

[3]Fan, C. S., and Metzger, D. E., "Effects of Channel Aspect Ratio on Heat Transfer in Rectangular Passage Sharp 180° Turn," ASME Paper 87-GT-113, 1987.

[4]Han, J. C., Chandra, P. R., and Lau, S. C., "Local Heat/Mass Transfer Distributions Around Sharp 180 Deg. Turns in Two-Pass Smooth and Rib-Roughened Channels," *Journal of Heat Transfer*, Vol. 110, 1988, pp. 91–98.

[5]Han, J. C., and Zhang, P., "Effect of Rib-Angle Orientation on Local Mass Transfer Distribution in a Three-Pass Rib-Roughened Channel," *Journal of Turbomachinery*, Vol. 113, 1991, pp. 123–130.

[6]Han, J. C., Zhang, Y. M., and Lee, C. P., "Augmented Heat Transfer in Square Channels with Parallel, Crossed, and V-Shaped Angled Ribs," *Journal of Heat Transfer*, Vol. 113, 1991, pp. 590–596.

[7]Park, J. S., Han, J. C., Huang, Y., and Ou, S., "Heat Transfer Performance Comparisons of Five Different Rectangular Channels with Parallel Angled Ribs," *International Journal of Heat and Mass Transfer*, Vol. 35, No. 11, 1992, pp. 2891–2903.

[8]Taslim, M. E., Li, T., and Kercher, D. M., "Experimental Heat Transfer and Friction in Channels Roughened with Angled, V-Shaped, and Discrete Ribs on Two Opposite Walls," *Journal of Turbomachinery*, Vol. 118, 1996, pp. 20–28.

[9]Ekkad, S. V., and Han, J. C., "Detailed Heat Transfer Distribution in Two-Pass Square Channels with Rib Turbulators," *International Journal of Heat and Mass Transfer*, Vol. 40, No. 11, 1997, pp. 2525–2537.

[10]Cho, H. H., Wu, S. J., and Kwon, H. J., "Local Heat/Mass Transfer measurements in a Rectangular Duct with Discrete Ribs," *Journal of Turbomachinery*, Vol. 122, 2000, pp. 579–586.

[11]Wagner, J. H., Johnson, B. V., and Hajek, T. J., "Heat Transfer in Rotating Passage with Smooth Walls and Radial Outward Flow," *Journal of Turbomachinery*, Vol. 113, 1991, pp. 42–51.

[12]Wagner, J. H., Johnson, B. V., and Kooper, F. C., "Heat Transfer in Rotating Passage with Smooth Walls," *Journal of Turbomachinery*, Vol. 113, 1991, pp. 321–330.

[13]Taslim, W. E., Rahman, A., and Spring, S. D., "An Experimental Investigation of Heat Transfer Coefficients in a Spanwise Rotating Channel with Two Opposite Rib-Roughened Walls," *Journal of Turbomachinery*, Vol. 113, 1991, pp. 75–82.

[14]Taslim, M. E., Bondi, L. A., and Kercher, D. M., "An Experimental Investigation of Heat Transfer in an Orthogonally Rotating Channel Roughened with 45 Deg Criss-Cross Ribs on Two Opposite Walls," *Journal of Turbomachinery*, Vol. 113, 1991, pp. 346–353.

[15]Han, J. C., Zhang, Y. M., and Kalkuehler, K., "Uneven Wall Temperature Effect on Local Heat Transfer in a Rotating Two-Pass Square Channel With Smooth Walls," *Journal of Heat Transfer*, Vol. 115, No. 4, 1993, pp. 912–920.

[16]Parsons, J. A., Han, J. C., and Zhang, Y. M., "Effects of Model Orientation and Wall Heating Condition on Local Heat Transfer in a Rotating Two-Pass Square Channel with Rib Turbulators," *International Journal of Heat and Mass Transfer*, Vol. 38, No. 7, 1995, pp. 1151–1159.

[17]Zhang, Y. M., Han, J. C., Parsons, J. A., and Lee, C. P., "Surface Heating Effect on Local Heat Transfer in a Rotating Two-Pass Square Channel with 60° Angled Rib Turbulators," *Journal of Turbomachinery*, Vol. 117, 1995, pp. 272–280.

[18]Dutta, S., and Han, J. C., "Local Heat Transfer in Rotating Smooth and Ribbed Two-Pass Square Channels with Three Channel Orientations," *Journal of Heat Transfer*, Vol. 118, 1996, pp. 578–584.

[19]Park, C. W., and Lau, S. C., "Effect of Channel Orientation of Local Heat (Mass) Distributions in A Rotating Two-Pass Square Channel with Smooth Walls," *Journal of Heat Transfer*, Vol. 120, 1998, pp. 624–632.

[20]Park, C. W., Yoon, C., and Lau, S. C., "Heat (Mass) Transfer in a Diagonally Oriented Rotating Two-Pass Channel with Rib-Roughened Walls," *Journal of Heat Transfer*, Vol. 122, 2000, pp. 208–211.

[21]Liou, T. M., Chen, M. Y., and Tsai, M. H., "Fluid Flow and Heat Transfer in a Rotating Two-Pass Square Duct with In-Line 90-deg Ribs," *Journal of Turbomachinery*, Vol. 124, 2002, pp. 260–268.

[22]Al-Hadhrami, L., and Han, J. C., "Effect of Rotation on Heat Transfer in Two-Pass Square Channels with Five Different Orientations of 45° Angled Rib Turbulators," *International Journal of Heat and Mass Transfer*, Vol. 46, 2003, pp. 653–669.

[23]Azad, G. S., Uddin, M. J., Han, J. C., Moon, H. K., and Glezer, B., "Heat Transfer in a Two-Pass Rectangular Rotating Channel with 45-Deg Angled Rib Turbulators," *Journal of Turbomachinery*, Vol. 124, 2002, pp. 251–259.

[24]Griffith, T. S., Al-Hadhrami, L., and Han, J. C., "Heat Transfer in Rotating Rectangular Cooling Channels (AR = 4) with Angled Ribs," *Journal of Heat Transfer*, Vol. 124, 2002, pp. 617–625.

[25]Lee, E., Wright, L. M., and Han, J. C., "Heat Transfer in Rotating Rectangular Channels with V-Shaped and Angled Ribs," *Journal of Thermophysics and Heat Transfer*, Vol. 19, No. 1, 2005, pp. 48–56.

[26]Al-Hadhrami, L., Griffith, T. S., and Han, J. C., "Heat Transfer in Two-Pass Rotating Rectangular Channels (AR = 2:1) with Five Different Orientations of 45° V-Shaped Rib Turbulators," *Journal of Heat Transfer*, Vol. 125, 2003, pp. 232–242.

[27]Cho, H. H., Kim, Y. Y., Kim, K. M., and Rhee, D. H., "Effects of Rib Arrangements and Rotation Speed on Heat Transfer in a Two-Pass Duct," ASME Paper 2003-GT-38609, 2003.

[28]Agarwal, P., Acharya, S., and Nikitopoulos, D. E., "Heat Transfer in 1:4 Rectangular Passages with Rotation," *Journal of Turbomachinery*, Vol. 125, 2003, pp. 726–733.

[29]Fu, W. L., Wright, M. L., and Han, J. C., "Heat Transfer in Two-Pass Rotating Rectangular Channels (AR = 1:2 and AR = 1:4) with 45 Deg Angled Rib Turbulators," *Journal of Turbomachinery*, Vol. 127, 2004, pp. 164–174.

[30]Wright, M. L., Fu, W. L., and Han, J. C., "Thermal Performance of Angled, V-Shaped, and W-Shaped Rib Turbulators in Rotating Rectangular Cooling Channels (AR = 4:1)," *Journal of Turbomachinery*, Vol. 126, 2004, pp. 604–614.

[31]Han, J. C., Park, J. S., and Lei, C. K., "Heat Transfer Enhancement in Channels with Turbulence Promoters," *Journal of Engineering for Gas Turbines and Power*, Vol. 107, 1985, pp. 628–635.

[32]Kline, S. J., and McClintock, F. A., "Describing Uncertainty in Single-Sample Experiments," *Mechanical Engineering*, Vol. 75, 1953, pp. 3–8.

[33]Al-Qahtani, M., Jang, Y. J., Chen, H. C., and Han, J. C., "Prediction of Flow and Heat Transfer in Rotating Two-Pass Rectangular Channels with 45-Deg Rib Turbulators," *Journal of Turbomachinery*, Vol. 124, 2002, pp. 242–250.

[34]Su, G., Teng, S., Chen, H. C., and Han, J. C., "Flow and Heat Transfer Computation in Rotating Rectangular Channels with V-Shaped Ribs," *Journal of Thermophysics and Heat Transfer*, Vol. 18, No. 4, 2004, pp. 537–547.